buildings

MDPI

Article

Comparison of Methods for Emissivity Influence Suppression on Thermographic Data

Lukáš Muzika *, Jiří Tesař, Michal Švantner, Jiří Skála and Petra Honnerová

New Technologies—Research Centre, University of West Bohemia, Univerzitní 8, 301 00 Plzeň, Czech Republic
* Correspondence: muzika@ntc.zcu.cz

Abstract: Emissivity is a crucial parameter for a quantitative thermography measurement. It influences measured temperature using an infrared camera. Typically, the emissivity is handled by infrared camera software but often for more complex tasks—e.g., setting and controlling the emissivity of individual pixels—a custom-made solution must be created. This can be especially beneficial for active thermography measurement and dynamic building inspection by infrared thermography as many surfaces of interest with different emissivity occur in thermographic data. In literature, one technique for suppressing emissivity occurs most often—the technique used by infrared camera manufacturers. Nonetheless, two other techniques are marginally mentioned. The most complex technique is the one used by infrared camera manufacturers, which allows many parameters to be set, but it is difficult to incorporate it into own solution. In contrast, the second one can be adapted easily, and it uses the relationship between emissivity and the fourth power of temperatures. The third one is a scarcely used technique that occurs for some active thermography measurements, in which a thermographic sequence in counts is divided by a frame when temperature equilibrium is reached. The main goal of this article is to compare these individual techniques from the point of view of the accuracy and possibility of use. The experiment showed that all three methods can be successfully used for the suppression of emissivity influence.

Keywords: emissivity; infrared thermography; thermographic measurement; thermographic inspection; thermographic testing

Citation: Muzika, L.; Tesař, J.; Švantner, M.; Skála, J.; Honnerová, P. Comparison of Methods for Emissivity Influence Suppression on Thermographic Data. *Buildings* **2023**, *13*, 69. https://doi.org/10.3390/buildings13010069

Academic Editor: Alessandro Cannavale

Received: 28 November 2022
Revised: 19 December 2022
Accepted: 23 December 2022
Published: 28 December 2022

1. Introduction

Thermographic cameras are increasingly used for building inspection. They are used for applications such as detecting thermal bridges [1,2], detection of insulation heterogeneities [3], moisture detection [4], and many more. Thermographic measurements can bring useful information for analyses of building structures' thermal transmittance [5,6] or in the modelling of thermal comfort in buildings [7]. Furthermore, thermographic cameras are being used for active thermography measurements in this field as well. The applications are, for example, detecting defects in timber [8], non-destructive quality evaluation of concrete structures [9], or the structural health monitoring of bridges [10]. Thermography methods are also successfully applied for an inspection of hidden elements of cultural heritage structures, as was presented, for example, in [11] or [12]. All of these infrared thermography applications more or less require solving the issue of the emissivity of the inspected surfaces.

Thermographic cameras measure infrared radiation intensity from an observed object. The radiation intensity can be subsequently converted to a temperature distribution. This effect is commonly used and most thermographic cameras typically display temperatures. The physic behind conversion from radiation to temperature is based on Planck's law from which Stefan–Boltzmann's law can be derived by wavelength integration [13]. This

law describes the radiation intensity of the black body depending only on the absolute temperature [13,14].

$$M^{BB}(T) = \int_0^\infty \frac{2\,\pi\,h\,{c_0}^2}{\lambda^5\left(e^{\frac{h\,c_0}{\lambda\,k\,T}}\right) - 1}\,d\lambda = \sigma\,T^4, \tag{1}$$

where M^{BB} is a radiation of the black body, h is Planck's constant, k is Boltzmann's constant, c_0 is the speed of light in vacuum, λ is wavelength, T is temperature in Kelvin, and σ is Stefan–Boltzmann's constant.

It should be clarified that a black body radiator is an ideal object for measurement by an infrared camera. Its total radiation is composed only of one component (absorbed radiation). Commonly, the object does not have the properties of the black body radiator. Therefore, a parameter called emissivity is used to relate a real object to the black body radiator. Emissivity is defined as the ratio of the radiation intensity of the real body to the radiation of the black body with the same temperature. Therefore, the value of emissivity can be from 0 to 1. Unfortunately, emissivity is not a constant. It depends on temperature, direction, wavelength, spectral band, and more [15].

From Equation (1), a relation for a real body can be derived.

$$M(T) = \varepsilon\,\sigma\,T^4, \tag{2}$$

where ε is emissivity.

In reality, radiation is detected via a matrix detector. Results from this detector are analog electrical values which are converted via analog/digital (A/D) convertor to data which are then processed digitally. It should be clarified that for the discovery of real radiation, digital values must be also calibrated. Typically, this is performed only when real temperatures need to be discovered. Raw data from cameras are signal values (often called object signal or counts) [14]. Temperature can be obtained by Equation (3) [13,16], which is sometimes called an RBFO equation.

$$T = \frac{B}{\ln\left(\frac{R}{W-O} + F\right)}, \tag{3}$$

where T is the temperature in Kelvin, O is offset, R is the system response of the infrared (IR) detector, B describes the spectral behavior of the system, F allows for an alignment of the non-linearity of the system, and W is the signal, which linearly corresponds with radiation intensity.

Equation (3) can be derived from Equation (1). The physical constants in Equation (1) are used for calculation; nonetheless, imperfections in IR camera manufacturing can lead to an imprecise result. This can be caused, for example, by the non-linearity of individual detectors and their different gain. Therefore, manufacturers tweak the conversion to reach the best results.

All constants R, B, F, and O are connected to an individual camera chip. Equation (3) can be used as-is for conversion from object signals (counts) to temperature for the ideal state. In this case, W is equal to the flux of radiation. In reality, other effects need to be taken into account, such as background temperature, atmospheric temperature, transmissivity coefficient, and emissivity. Figure 1 shows individual effects that influence measured temperature. Measured flux by an IR camera is composed of the radiant flux originating from the surface of the measured object, the radiation heading to the detector after reflection from the measured surface, and the radiation of the atmosphere between the measured object and the device detector [17]. Furthermore, lenses or protective glass also influence measured temperature. Its effect can be neglected when calibration is performed with it. The problem can occur when lenses or protective glass are switched; this is also the reason why manufacturers give different calibration files for different lenses.

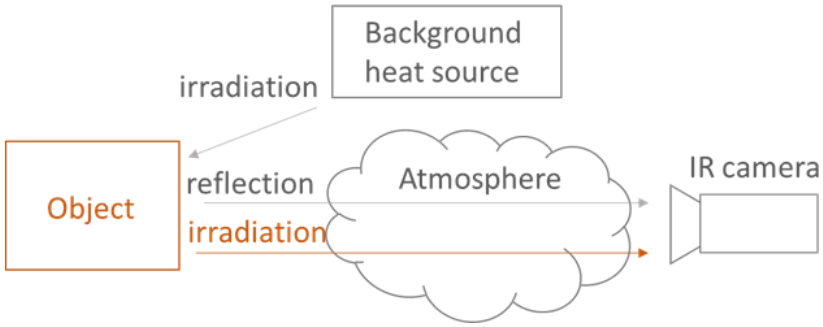

Figure 1. General measurement setup.

Mathematically, the flux of the object is expressed as [13]:

$$W_{obj} = \frac{W_{meas}}{\tau_{atm} \cdot \varepsilon} - \frac{1-\varepsilon}{\varepsilon} \cdot W_{bkg} - \frac{1-\tau_{atm}}{\tau_{atm} \cdot \varepsilon} \cdot W_{atm}, \quad (4)$$

where W_{obj} is the flux originating from the object, τ_{atm} is transmission coefficient of the atmosphere, W is the flux, *bkg* stands for the background, *atm* stands for the atmosphere, and *meas* stands for measured.

Sometimes Equation (4) contains a member that describes the behavior of the lens/objective (window). This member can be neglected when RBFO constants are derived for the whole measurement device (with objective or lenses).

W is calculated via the inverse relation stated in Equation (3). After the calculation of each W, the W of the object is calculated. This W is used in Equation (3), and then the real temperature is calculated. In many applications, the relation is simplified. The transmissivity of the atmosphere is set to 1. Then, relation is:

$$W_{obj} = \frac{W_{meas}}{\varepsilon} - \frac{1-\varepsilon}{\varepsilon} \cdot W_{bkg}, \quad (5)$$

where W_{bkg} is calculated via relation from Equation (6)

$$W_{bkg} = \frac{R}{e^{\frac{B}{T_{bkg}}} - F} + O. \quad (6)$$

Either way, when an IR camera is used, a user does not need to know mentioned relations, because camera software calculates everything on its own. The user only needs to set proper parameters (emissivity, background temperature, transmissivity, etc.).

Background temperature and atmospheric temperature are commonly set to the surrounding temperature, which can be measured with a thermometer. In special cases, such as when a reflection of a hotter background object can be seen in a thermogram, the background temperature is set to the temperature of this hot background object. Atmospheric transmissivity is set to 1 as it usually influences an object's apparent temperature only when far objects are measured (>10 m from an IR camera) or in the case of specific atmospheric conditions (e.g., in the case of high humidity) [13].

The biggest problem is that RBFO constants are often unknown and emissivity is also often unknown. There are ways how to determine emissivity. Some of them need special equipment (for example, Fourier transform infrared (FTIR) spectrometer). A much simpler method can be used in real-life applications such as the method of known temperature and the method of known emissivity [13]. In the method of known temperature, the real temperature (reference temperature) is known and, according to that, the measured temperature is adjusted via emissivity value. This way, the emissivity value is discovered and can be used for another measurement. In the case of the method of known emissivity [13], part of the specimen is covered by paint of known emissivity and the unknown emissivity of

the unpainted part is calculated based on a temperature equality assumption (above room temperature).

Typically, IR camera software allows for setting the emissivity of the whole image. More sophisticated software allows for manually set zones (for example, circle, and rectangle) of different emissivity. Nonetheless, for more complicated shapes or many different surfaces with different emissivity, this approach of setting zones is hardly feasible. For such applications, custom-made solutions are often needed.

Normally, the commonly used principle of emissivity influence suppression is often unusable because of the fact that many parameters specific to the individual infrared camera are unknown (e.g., RBFO). Alternative approaches are somehow mentioned in the literature, but no direct comparison was made. This article focuses on this unique comparison. Verification is performed for both mid and long wavelength thermographic cameras to demonstrate a usability of the methods in different wavelength ranges. Furthermore, a technique for emissivity suppression with minimum information about the measured object is described.

2. Methods

In this study, 3 different methods of emissivity correction were performed. The results of each method can be a thermographic sequence or one thermogram, where the influence of emissivity is suppressed. For a thorough demonstration of the proposed techniques, thermographic sequences were compared. The raw data contains a frame where there is an equal temperature. From this image, emissivity is calculated. Emissivity, the surrounding temperature, and reflected temperature are expected to be constant during the whole time.

2.1. Method 1

The influence of emissivity is corrected in the same way as in software provided by IR camera manufacturers (the method is described in the introduction). First, R, B, F, and O constants must be obtained to convert measured temperature to object signal. These parameters can be obtained from the Software Development Kit (SDK) of the camera or can be derived (less precisely) from Planck's law (Equation (1))

$$R = \frac{2 \cdot h \cdot c^2}{\lambda^5}, \tag{7}$$

where λ is the peak spectral sensitivity,

$$B = \frac{h \cdot c}{\lambda \cdot k}. \tag{8}$$

Symbols in Equations (7) and (8) are explained under Equation (1). When constants R and B are derived from Planck's law, F is set to 1 (there is 1 in the denominator in Equation (1)), and O is set to zero (there is no offset when deriving Planck's law).

Values obtained from the SDK and from Planck's law are commonly different. Manufacturers tune those parameters specifically to each camera to reach the best performance.

Then W_{bkg} is calculated via Equation (6). Derived R, B, F, and O values and background temperature in Kelvin are used for this purpose. The same approach can be used for the calculation of W_{refl}.

Real radiance is calculated via Equation (4), where W_{meas} is the measured radiance (without any correction; if radiance was measured with emissivity correction, this correction must be included in the equations). Then, a reverse RBFO equation is used (Equation (3)) and the corrected temperature is calculated.

Emissivity can be calculated according to Equation (9), when W_{obj} is known,

$$\varepsilon = \frac{W_{meas} - \tau_{atm} \cdot W_{bkg} - (1 - \tau_{atm}) \cdot W_{atm}}{\tau_{atm} \cdot (W_{obj} - W_{bkg})}. \tag{9}$$

The scheme of method 1 is shown in Figure 2. The sequence in the scheme contains 3 frames. The last frame is the frame where the same temperate is in each pixel (Equilibrium frame). The sequence in °C is converted to object signal (OS) via Equation (6) (with relevant subscripts). Background temperature and atmospheric temperature are converted as well via Equation (6). The emissivity map is calculated from the equilibrium frame and OS values corresponding to the background, atmospheric temperature, and the temperature in equilibrium according to Equation (9). Equilibrium temperature can be measured, for example, by thermocouple. The corrected sequence in OS is calculated via Equation (4). Conversion to °C is conducted by Equation (3). It should be clarified that values in the scheme are only for illustration purposes. In addition, special consideration should be focused on input data. In some cases, the sequence is already measured with default emissivity (e.g., 0.92, for every pixel). In this case, obtained values must be converted first to an uncorrected sequence (i.e., emissivity 1). It should also be clarified that conversion with the RBFO equation (Equation (3)) and inverse RBFO equation (Equation (6)) works in Kelvins (°C or °F must be transformed to K).

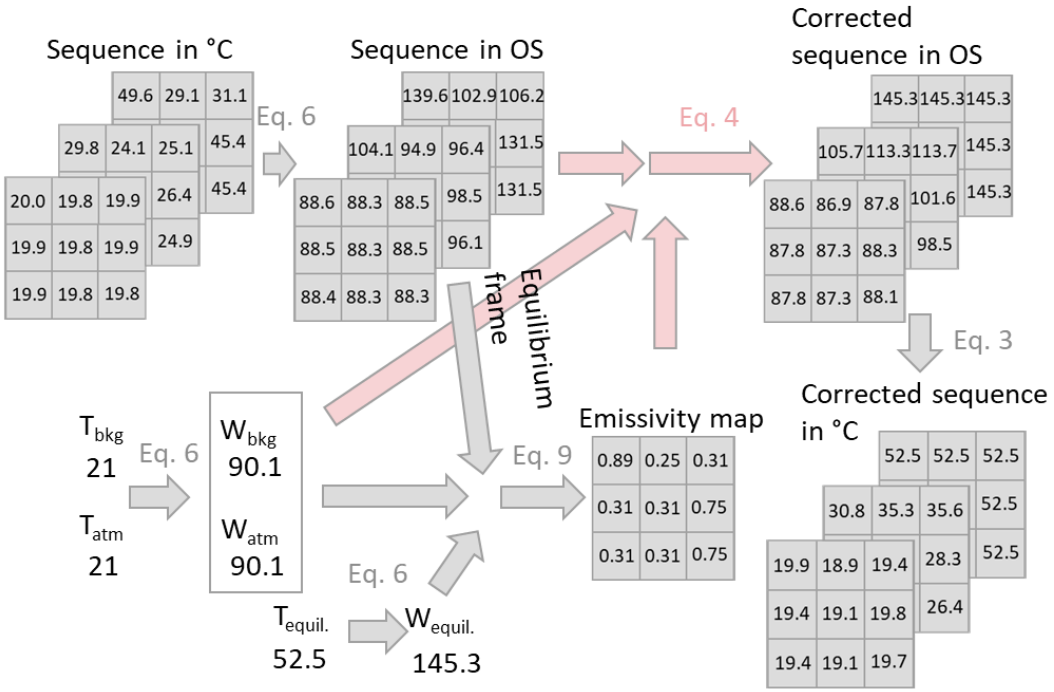

Figure 2. Scheme of method 1.

2.2. Method 2

Influence of emissivity is corrected via relation (10) [18]

$$T_{total} = \sqrt[4]{\frac{T_{meas}^4 - (1-\varepsilon)\cdot T_{bkg}^4}{\varepsilon}}, \tag{10}$$

where T_{obj} is real temperature, T_{meas} is measured temperature, and T_{bkg} is background temperature.

This is an equation that is valid for all wavelengths based on Stefan–Boltzmann's law. Because IR cameras do not measure in the whole wavelength range, the result should be expected to be worse than with method 1. Nonetheless, usage of this relationship is much more straightforward.

Emissivity can be calculated via Equation (11)

$$\varepsilon = \frac{T_{meas}^4 - T_{bkg}^4}{T_{obj}^4 - T_{bkg}^4}. \tag{11}$$

The scheme of method 2 is in Figure 3. The emissivity map is calculated via Equation (11) from the equilibrium frame and background temperature and equilibrium temperature. The corrected sequence is calculated via Equation (10).

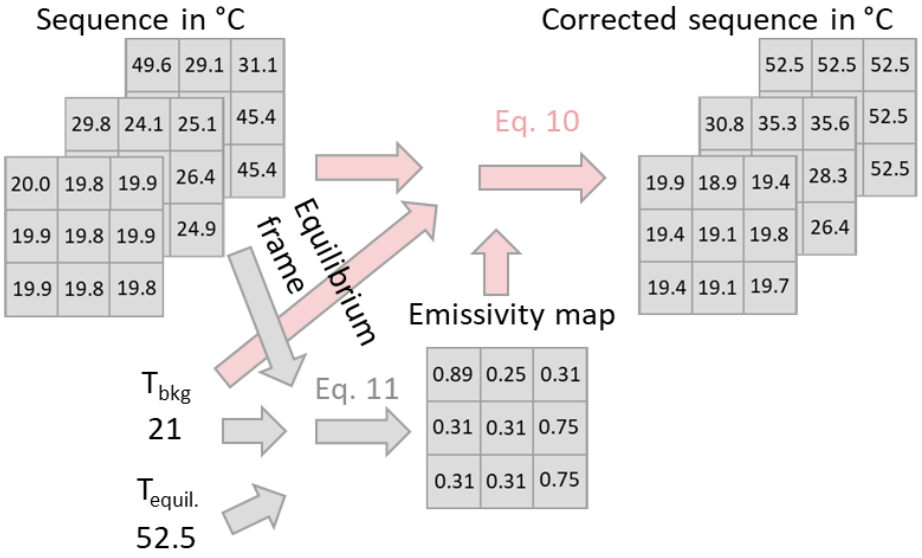

Figure 3. Scheme of method 2.

2.3. Method 3

Method 3 is based on Equation (5). First, the temperature must be converted to an object signal (or must be measured in object signal units). This method assumes that the reflected temperature is the same for the whole measurement so that the whole part of the equation is constant. Thereby, it leads to Equation (12)

$$\Delta W_{obj} = \frac{\Delta W_{meas}}{\varepsilon}. \tag{12}$$

This equation can be written as

$$W_{obj}(t_x) - W_{obj}(0) = \frac{W_{meas}(t_x) - W_{meas}(0)}{\varepsilon}, \tag{13}$$

where Δ is expressed as a difference between the measured signal or real radiance in time x and the measured signal or real radiance in time 0 (first frame subtraction).

When W_{obj} is the same for a whole captured frame (the measured process is in thermal equilibrium). Emissivity can be obtained by relationship (14)

$$\varepsilon = \frac{W_{meas}(t_e) - W_{meas}(0)}{W_{obj}(t_e) - W_{obj}(0)}, \tag{14}$$

where t_e is the time of equilibrium.

The sequence, in which the effect of emissivity is suppressed, can be calculated via Equation (15). Nonetheless, this result cannot be converted back to temperature. This type of suppression was used, for example, in [19,20] for the suppression of emissivity for active thermography measurements. In this form, the emissivity influence is suppressed in the whole thermographic sequence in object signals which may be sufficient for many applications. The benefit is that for the calculation, no knowledge of emissivity nor temperature in equilibrium was needed.

$$W_{ES}(t_x) = \frac{W_{meas}(t_x) - W_{meas}(0)}{W_{meas}(t_e) - W_{meas}(0)} \tag{15}$$

We propose using the relation described in Equation (6) to be able to convert radiation back to temperature. For these purposes, the real flux (or temperature) in time of equilibrium must be known. ΔW_{obj} at any time can be calculated via (16)

$$\Delta W_{obj}(t_x) = \frac{W_{meas}(t_x) - W_{meas}(0)}{W_{meas}(t_e) - W_{meas}(0)} \cdot \Big(W_{obj}(t_e) - W_{obj}(0) \Big), \tag{16}$$

W_{obj} is then

$$W_{obj}(t_x) = \Delta W_{obj}(t_x) + W_{obj}(0) \tag{17}$$

The flux can be converted back to temperature via the RBFO equation.

The scheme of method 3 is in Figure 4. Firstly, the subtraction of the first image is conducted for a sequence in OS. Division by the frame, when there is temperature equilibrium, follows. The influence of emissivity is already suppressed in the resulting sequence. Additional steps follow due to the conversion to degrees Celsius. The resulting sequence is multiplied by the difference between the real temperature in equilibrium and the initial temperature (initial temperature of the specimen). Initial radiance is added to the sequence. The corrected sequence in °C is calculated via Equation (6).

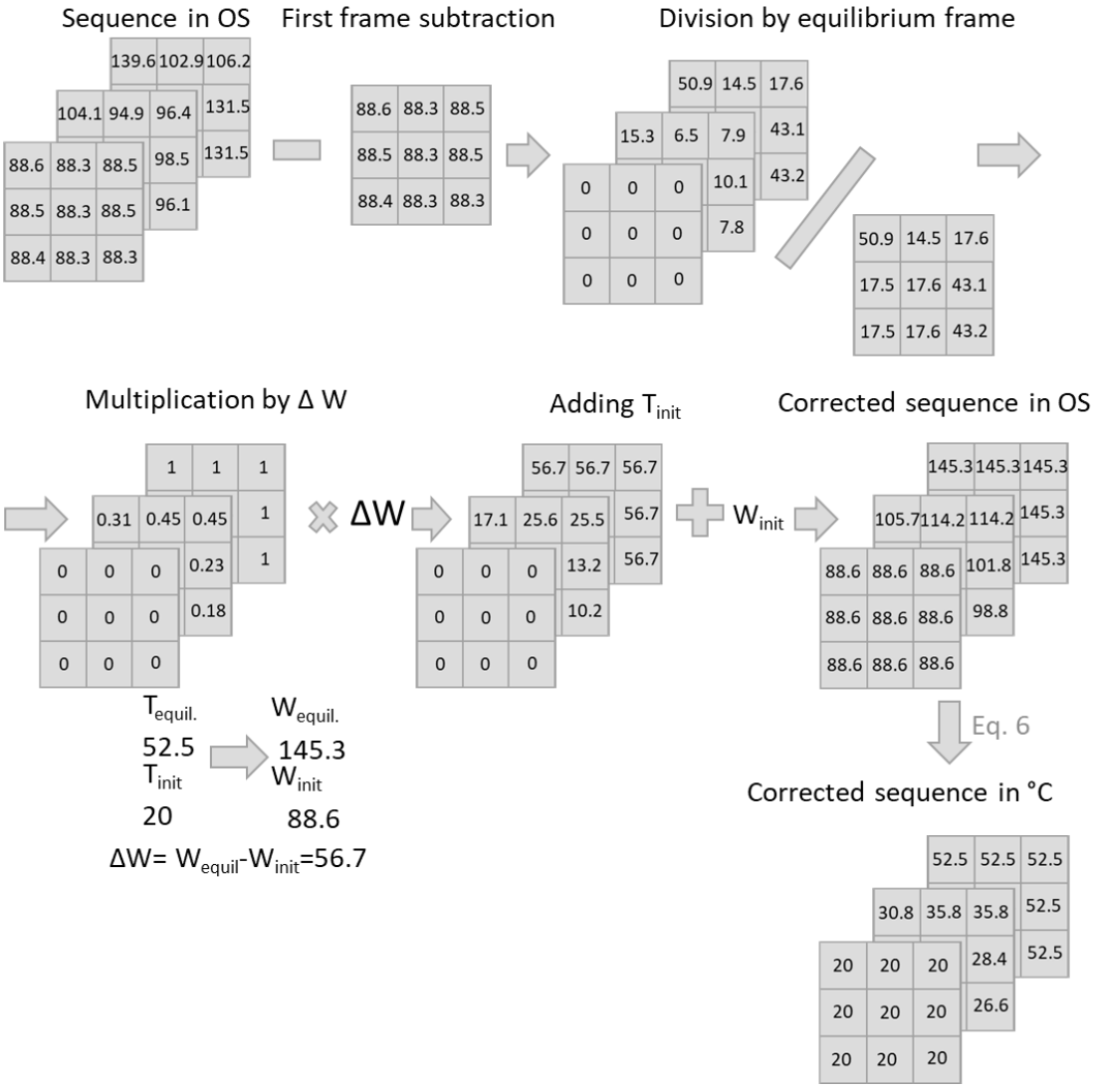

Figure 4. Scheme of method 3.

3. Experimental Program

To determine the suitability of the described methods, thermographic measurement of the heating of samples with different emissivities on a hot plate was performed. Four specimens with dimensions 100 × 50 × 1.5 mm made of AISI 304 steel were inspected. Specimens had different emissivity. The emissivity change of three specimens (A1–A3) was performed by laser with different processing parameters (different oxide layers were created). The last specimen (A4) was sprayed with special thermographic paint (LabIR-HERP-HT-MWIR-BK-11) with known emissivity. The measurement from A4 was considered to be the reference. Heating was performed in four steps, which followed each other. First, specimens were placed on a hot plate (room temperature). Next, the heating at 30 °C started. This temperature was held for 15 min. Then, the same procedure continued at 50 °C, 70 °C, and 90 °C.

The whole procedure was captured by two infrared cameras. The first camera was bolometric long-wavelength (LWIR) camera FLIR A615 (wavelength range 7.5–14 μm, Noise Equivalent Temperature Difference (NETD) ≤ 50 mK), which represents the most commonly used IR cameras. The second one was a mid-wavelength (MWIR) high-speed high-sensitivity camera, FLIR A6751 (a cooled InSb detector type IR camera, wavelength range 3–5 μm, NETD ≤ 20 mK). The heating was also measured by one thermocouple for verification of the measured temperature. Before this experiment, the homogeneity of heating by hot plate was verified by several thermocouples, which showed the difference in the range of tenths of a degree Celsius. Therefore, the heating was considered homogeneous over the entire hot plate.

The scheme and photography of the measurement configuration are in Figure 5.

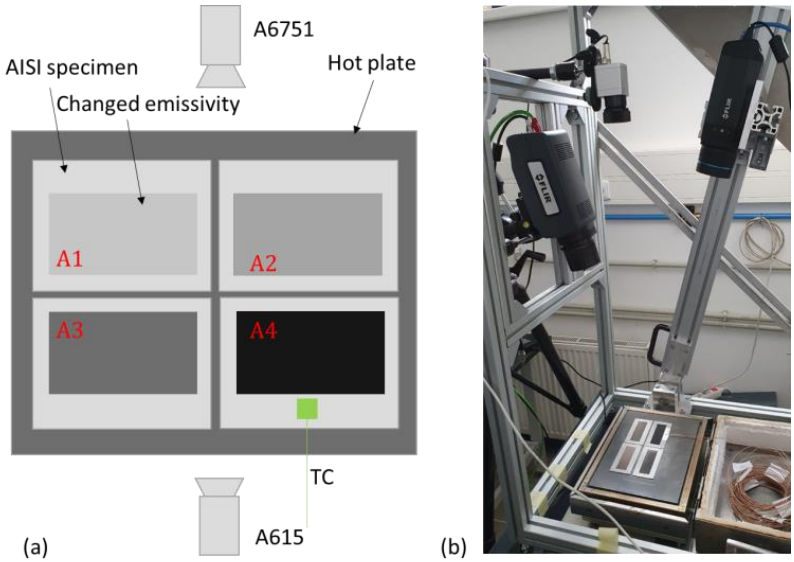

Figure 5. Measurement setup (**a**) scheme, (**b**) photography.

4. Results and Discussion

The suitability of these methods for suppression of emissivity influence was determined by comparing the time–temperate curve from zones A1–A3 with reference area A4. Each time, the temperature curve should look similar to A4. Preliminary determination of emissivity was performed with spectrometer Nicolet 6700. The result is in Figure 6.

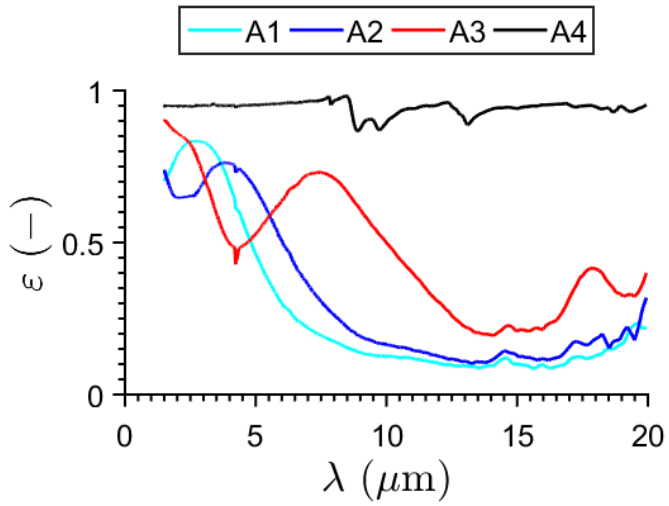

Figure 6. Emissivity of the specimen for different wavelength.

Emissivity measurement showed similar emissivity in the whole measurement range for specimen A4. This specimen was painted with high emissivity thermographic paint, thereby this result was expected. Specimens made by laser processing (A1–A3) had lower emissivity in higher wavelengths. Thus, for the mid-wave IR camera (FLIR A6751), the lowest emissivity should have specimen A3, then A1, A2, and A4. For the long-wave IR camera, the lowest emissivity should have specimen A1, then A2, A3, and A4.

Measurement results for camera FLIR A615 (long-wave) are displayed in Figure 7. Figure 7a displays the raw measured temperature (average values from A1, A2, A3, and A4; the zones from which average values are calculated are slightly smaller than real zones to suppress the influence of different emissivity on the edges of zones). Figure 7c shows emissivity correction performed by method 1. The emissivity map was calculated when the equilibrium on the hot plate was set to 90° C or, more specifically, the frame when the 90 °C was stabilized (in half of the 15-min interval). The reflected temperature was measured with the reflector method [13]. A rumpled and re-flattened sheet of aluminum foil was placed in the same place as the measured object. The emissivity was set to 1. Then, the apparent temperature was measured. This procedure was performed three times and the result was averaged. The temperature was the same as the atmospheric (room) temperature, which was 20.1 °C. Humidity was 55%. Laboratory room conditions were constant during measurement.

As the results show, emissivity correction failed for lower temperatures. The lower the emissivity of the area was, the bigger the difference compared to the reference area was visible. The average values of emissivity for A1–A4 evaluated from the emissivity map were 0.18, 0.19, 0.51, and 0.92, which means that A1 and A2 were highly reflective and standard emissivity correction did not work. Area A3 had significantly higher emissivity than A1 and A2 and the correction was better, but still not perfect. The main reason why emissivity correction failed was the different reflected temperature. The background temperature differed for each pixel. An additional correction had to follow. Instead of fine-tuning the reflected temperature for each pixel, which is impractical for real-life applications, a different approach was used. The first image was subtracted, and the initial temperature (measured by the thermocouple) was added for the whole sequence. This allowed us to see temperature changes directly connected with heating by the hot plate. The curves are displayed in Figure 7b. Subsequent emissivity correction for the adjusted sequence is in Figure 7d. In this case, time–temperature curves are similar for each specimen. The influence of emissivity was successfully suppressed in this case.

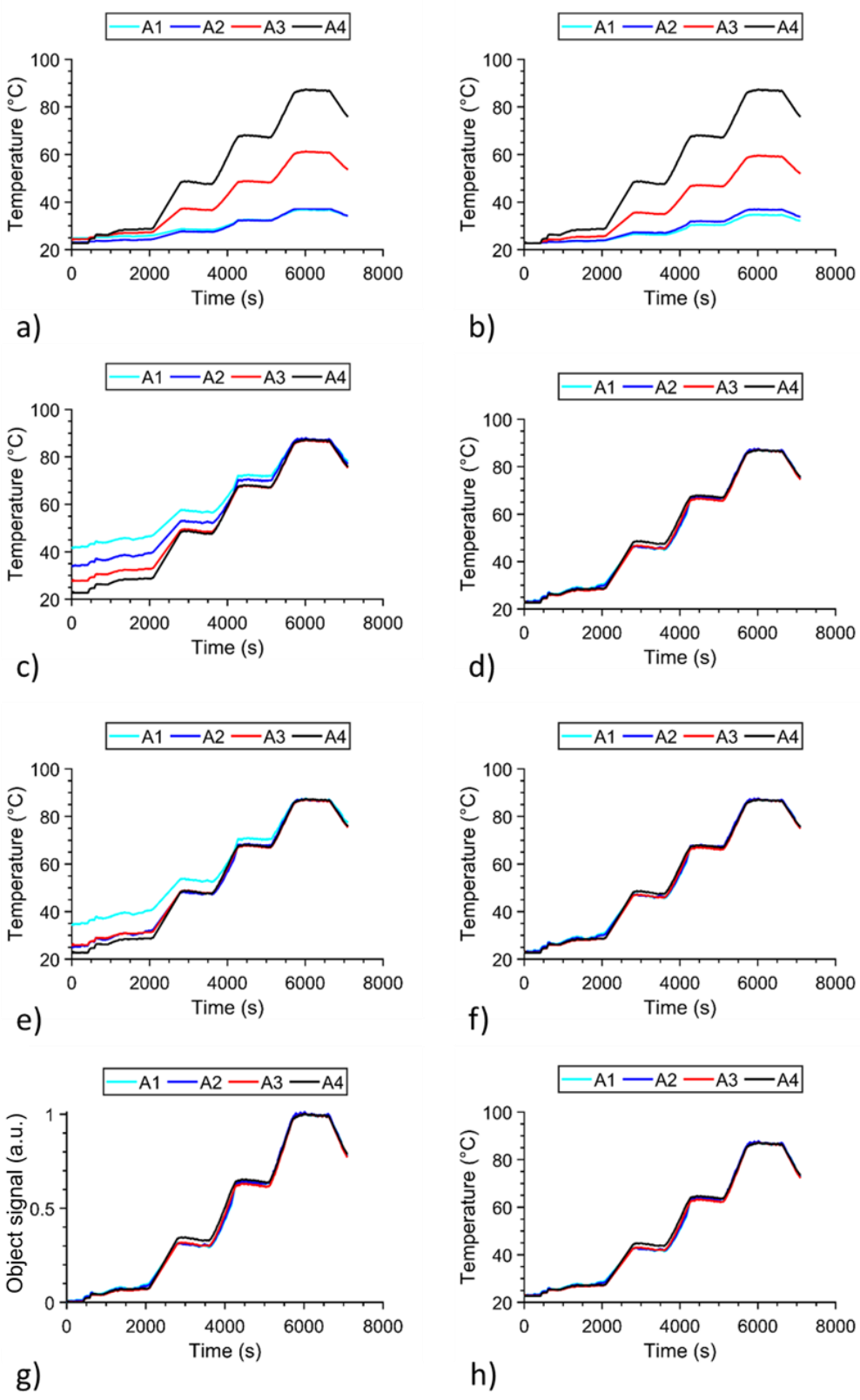

Figure 7. Measurement result for FLIR A615 (LWIR): (**a**) raw data (whole image emissivity 0.92), (**b**) raw data − 1st image + Tinit (emissivity 0.92), (**c**) emissivity correction method 1 of (**a**), (**d**) emissivity correction method 1 of (**b**), (**e**) emissivity correction method 2 of (**a**), (**f**) v correction method 2 of (**b**), (**g**) emissivity correction method 3 in OS, (**h**) emissivity correction method 3 in °C.

The result of method 2 for raw data is in Figure 7e. As can be seen, temperature values were corrected slightly better than in the case of method 1 on raw data. The temperature was corrected well for A2–A4 at 50 °C, 70 °C, and 90 °C. When correction is applied to adjusted data (Figure 7b), emissivity correction was successful.

The results of method 3 in OS are in Figure 7g. The same frame that was used for creating emissivity maps for methods 1 and 2 (and with subtracted first frame) in counts was used for the correction. As can be seen, the time OS curves are almost identical. In this case, suppression of emissivity was performed only with knowledge of when thermal equilibrium is reached. It should be clarified that this process can be performed only for object signal values because radiation and temperature do not have a linear dependency. Figure 7h shows that it is possible to convert the OS value back to temperature. Nonetheless, correction must be performed with Equations (16) and (17), which means that initial temperature (radiance) must be known as well as the constants of the RBFO equation and temperature (radiance) at equilibrium.

All three methods were able to suppress the influence of different emissivity for the long-wave IR camera FLIR A615.

Results from the mid-wave IR camera are shown in Figure 8. First, raw data (Figure 8a) shows that specimen A3 has the lowest emissivity (measured temperature is the lowest). This corresponds with the measurement performed with the spectrometer (Figure 6). Furthermore, when correction method 1 is applied to raw data, emissivity was corrected successfully. No first image subtraction was needed. The emissivity map showed these average values from A1–A4: 0.61, 0.71, 0.54, 0.92. Values of emissivity are much higher than in the case of measurement with long-wave IR camera FLIR A615. Therefore, background and atmospheric temperature do not have such a significant effect on the results. For completeness, in the first image, subtraction and addition of initial temperature were performed either way (Figure 8b). Correction is in Figure 8d.

The results of method 2 are in Figure 8e,f. The method shows good emissivity suppression in both cases (raw data, adjusted data).

As can be seen in Figure 8g,h, method 3 also provides good emissivity suppression.

Table 1 shows the comparison of methods. As was mentioned before, the raw measurement from specimen A4 was chosen as the reference (the whole time–temperature curve). The emissivity of A4 was known (0.92, paint) and emissivity was the same as the default for the used software, which means that the measured temperature should be the same as the real temperature. The absolute (abs) difference between the time–temperature curve from every area and the reference time–temperature curve was calculated. Furthermore, the standard deviation (STD) was calculated.

The most suitable method for suppression of emissivity influence on temperature data was the adjusted method 2 for the long-wave IR camera (the average absolute difference was 0.34 °C, bold in Table 1 for A615) and the adjusted method 1 for the mid-wave IR camera (the average absolute difference was 0.21 °C, bold in Table 1 for A6751). The temperature differences between different methods for the mid-wave IR camera are small. Adjusted method 1 reached almost the same results as method 3. The worst was method 2 with an average absolute difference of 0.63 °C. As can be seen, the standard deviation was smaller than for the long-wave camera, which is caused by better NETD compared to the long-wave camera.

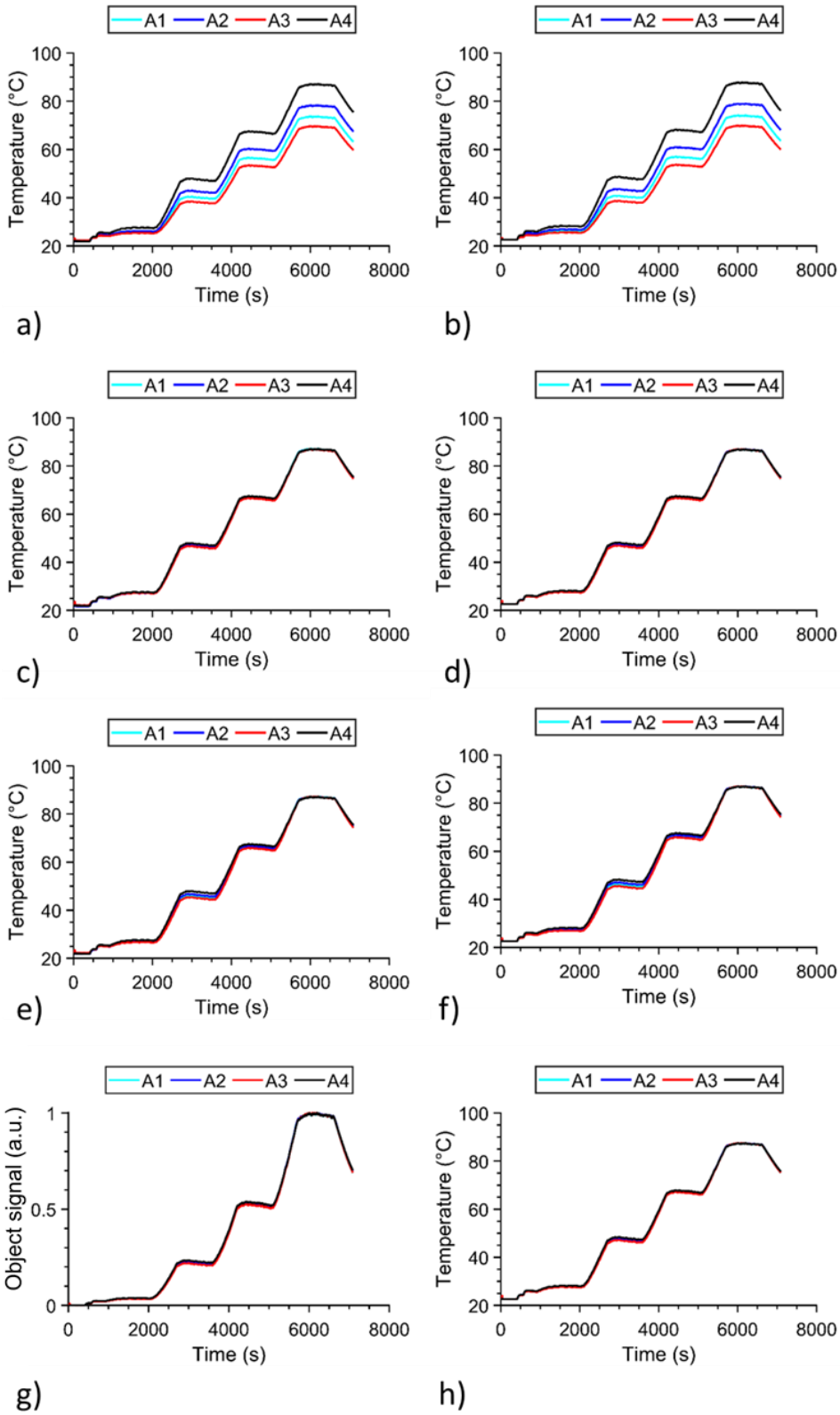

Figure 8. Measurement result for FLIR A6751 (MWIR): (**a**) raw data (whole image emissivity 0.92), (**b**) raw data − 1st image + Tinit (emissivity 0.92), (**c**) emissivity correction method 1 of (**a**), (**d**) emissivity correction method 1 of (**b**), (**e**) emissivity correction method 2 of (**a**), (**f**) emissivity correction method 2 of (**b**), (**g**) emissivity correction method 3 in OS, (**h**) emissivity correction method 3 in °C.

Table 1. Comparison of methods, differences between individual time–temperature curves and the reference curve (°C). Best average results for each camera are in bold.

		A615					A6751				
		A1	**A2**	**A3**	**A4**	**Average**	**A1**	**A2**	**A3**	**A4**	**Average**
Method 1	mean abs difference	8.49	4.91	1.38	0	3.7	0.37	0.35	0.57	0	0.32
	mean abs STD	7.14	4.19	1.13	0	3.12	0.34	0.19	0.45	0	0.25
Method 1 adjusted	mean abs difference	0.55	0.58	0.98	0.15	0.56	0.22	0.02	0.37	0.21	**0.21**
	mean abs STD	1.44	1.25	0.79	0.08	0.89	0.45	0.32	0.51	0.3	0.4
Method 2	mean abs difference	5.27	0.7	0.72	0	1.67	0.82	0.59	1.12	0	0.63
	mean abs STD	4.57	1.44	1.43	0	1.86	0.71	0.44	0.94	0	0.52
Method 2 adjusted	mean abs difference	0.21	0.24	0.76	0.15	**0.34**	0.71	0.28	1.05	0.24	0.57
	mean abs STD	1.26	1.07	0.62	0.08	0.76	0.72	0.46	0.95	0.31	0.61
Method 3	mean abs difference	0.42	0.45	0.84	0.02	0.44	0.03	0.25	0.12	0.44	0.21
	mean abs STD	1.43	1.25	0.76	0	0.86	0.37	0.22	0.46	0.13	0.23

Unadjusted methods 1 and 2 for the long-wave IR camera showed the biggest difference from the reference. These methods are unsuitable, which was caused by low values of emissivity for A1 and A2. For those specimens, the surroundings significantly influenced the measurement and follow up emissivity influence suppression. In case the data are adjusted (first image subtraction and adding initial temperature), both methods were able to suppress the influence of emissivity.

Method 1 is a common method when dealing with different emissivity. This method was meant as a reference method and it provided overall good results. Its biggest advantage is that it is the most universal and complex. Nonetheless, it is difficult to incorporate it into a custom-made solution.

Interestingly, method 2, which is based on the Stefan–Boltzmann law for every wavelength, also showed good results. The method achieved better results for the long-wave IR camera, which is probably caused by the fact that this camera covers a bigger wavelength spectrum. The advantage is that it can easily be adapted and there is no need to convert from temperature to object signal, and vice versa (the other two methods work with object signal, but this method works only with temperatures). Thereby, there is no need to know the constant from the RBFO equation. It should be clarified that this method achieved a good result for the long-wave IR camera, but a not so good result for the mid-wave IR camera. It can be expected that for the short-wave IR camera, the method would provide even worse results because those cameras cover the smallest wavelength range. The method is the easiest to implement out of the compared methods and it can be a great tool for fast suppression of emissivity influence.

Method 3 is especially appealing for the suppression of emissivity influence when not much information about real temperature and emissivity is known. For some applications, e.g., qualitative thermography, the temperature does not have to be known and then the influence of emissivity can be suppressed just with the division of measured sequence with the frame, where the temperature is the same for the whole frame, as was demonstrated in [20,21]. If additional information is known (RBFO constant, initial temperature, equilibrium temperature), the temperature can be calculated. The experiment shows that method 3 is fully usable for the suppression of emissivity influence. It can be extremely useful for measurement where values in object signals can be used (e.g., detecting missing insulation or detecting humidity). The method achieved very good results for both cameras (it was always second in accuracy). It can be implemented very fast in object signals. In the case of using temperature values in K, the method is more complicated than method 2, but is still less complicated than method 1. This means that implementation time is second

best. The usability of the technique is limited. The equilibrium frame must be known. This makes the technique usable mostly just for dynamic measurement.

5. Conclusions

Three methods for the suppression of emissivity influence were introduced and compared. The methods allow for the set-up of different emissivity for individual pixels. This can be used, for example, when part of the test object is covered with paint, which caused the temperature to appear different due to different emissivity.

The methods were experimentally investigated. Experiments were performed in the mid-wave IR spectrum and the long-wave IR spectrum to show the feasibility for the most common IR cameras. It was shown that the standard emissivity correction method (method 1) could be replaced by both suggested alternative methods. It should be clarified that in order for all methods to work, the surrounding temperature and emissivity must remain constant during measurement.

The results confirmed that for low emissivity surfaces, surrounding reflection has a dominant effect. The methods failed, especially for lower temperatures, due to the inability to set proper parameters of the surrounding. It was shown that this obstacle can be eliminated when an image before the start of the monitored process is subtracted from the measured sequence. In this way, only the phenomenon is evaluated. This procedure is applicable only for dynamic measurement.

After this adjustment, the method derived from the Stefan–Boltzmann law (method 2) showed very good results for the long-wave IR camera. The average difference between the corrected time–temperature curve and the reference curve was 0.34 °C (the best of the three methods). The method did not perform that well for the mid-wave IR camera with an average difference of 0.57 °C (the worst of the three methods). Nonetheless, the method could still be viable for less demanding applications, where only big temperature differences must be recognized. The biggest advantage of method 2 is its simplicity. There is no need for the conversion between object signals and temperature values, thus it can be implemented rapidly.

The experiment showed good usability of the method, where a thermographic sequence in counts is divided by a frame when temperature equilibrium is reached (method 3). The method showed the second-best result with an average difference from reference 0.21 °C for mid-wave IR and 0.43 °C for long-wave IR. The method is especially beneficial for measurement where there is no need to work in real temperature values, and where object signal values are sufficient (e.g., detection of missing insulation, active thermography measurements). In this case, the method does not need any information about real temperature, and the measurement must only contain a frame with thermal equilibrium (higher than surrounding temperature). Nonetheless, if additional information is known, real temperature values can be retrieved.

The general conclusion of the experiment is that all three methods can be successfully used for the suppression of emissivity influence. The differences in results obtained by the analyzed methods were not too significant (less than 1 °C); however, the significant differences are in the implementation of the individual methods. Some IR cameras do not provide a raw object signal, only temperature values. In this case, method 2 is suitable because it does not require conversion to the object signal. In contrast, active thermography uses the object signal, and precise temperature values are usually not required. However, emissivity influence suppression can still be useful, and method 3 can then be used. Method 1 is a general-purpose method, but its applicability and implementation depend on the SDK capabilities of different IR cameras.

Author Contributions: Conceptualization, L.M. and M.Š.; methodology, L.M. and J.T.; software, J.S.; validation, M.Š. and J.T.; investigation, J.T. and P.H.; resources, M.Š.; data curation, L.M.; writing—original draft preparation, L.M., J.T. and M.Š.; writing—review and editing, M.Š.; visualization, L.M. and J.S. All authors have read and agreed to the published version of the manuscript.

Funding: This research was funded by the ERDF project "LABIR-PAV/Pre-application research of infrared technologies" Reg. No. CZ.02.1.01/0.0/0.0/18_069/0010018.

Data Availability Statement: Data available on request from the authors.

Conflicts of Interest: The authors declare no conflict of interest.

References

1. Sfarra, S.; Cicone, A.; Yousefi, B.; Ibarra-Castanedo, C.; Perilli, S.; Maldague, X. Improving the detection of thermal bridges in buildings via on-site infrared thermography: The potentialities of innovative mathematical tools. *Energy Build.* **2019**, *182*, 159–171. [CrossRef]
2. Šadauskienė, J.; Ramanauskas, J.; Krawczyk, D.A.; Klumbytė, E.; Fokaides, P.A. Investigation of Thermal Bridges of a New High-Performance Window Installation Using 2-D and 3-D Methodology. *Buildings* **2022**, *12*, 572. [CrossRef]
3. Balaras, C.; Argiriou, A. Infrared thermography for building diagnostics. *Energy Build.* **2002**, *34*, 171–183. [CrossRef]
4. Barreira, E.; Almeida, R.M.; Simões, M.L.; Rebelo, D. Quantitative infrared thermography to evaluate the humidification of lightweight concrete. *Sensors* **2020**, *20*, 1664. [CrossRef]
5. Gaši, M.; Milovanović, B.; Gumbarević, S. Comparison of infrared thermography and heat flux method for dynamic thermal transmittance determination. *Buildings* **2019**, *9*, 132. [CrossRef]
6. Lu, X.; Memari, A.M. Comparison of the Experimental Measurement Methods for Building Envelope Thermal Transmittance. *Buildings* **2022**, *12*, 282. [CrossRef]
7. Ghahramani, A.; Xu, Q.; Min, S.; Wang, A.; Zhang, H.; He, Y.; Merritt, A.; Levinson, R. Infrared-Fused Vision-Based Thermoregulation Performance Estimation for Personal Thermal Comfort-Driven HVAC System Controls. *Buildings* **2022**, *12*, 1241. [CrossRef]
8. Kucharska, M.; Jaskowska-Lemańska, J. Active thermography in diagnostics of timber elements covered with polychrome. *Materials* **2021**, *14*, 1134. [CrossRef] [PubMed]
9. Zheng, Y.; Wang, S.; Zhang, P.; Xu, T.; Zhuo, J. Application of Nondestructive Testing Technology in Quality Evaluation of Plain Concrete and RC Structures in Bridge Engineering: A Review. *Buildings* **2022**, *12*, 843. [CrossRef]
10. Kromanis, R.; Kripakaran, P. SHM of bridges: Characterising thermal response and detecting anomaly events using a temperature-based measurement interpretation approach. *J. Civ. Struct. Health Monit.* **2016**, *6*, 237–254. [CrossRef]
11. Glavaš, H.; Hadzima-Nyarko, M.; Buljan, I.H.; Barić, T. Locating hidden elements in walls of cultural heritage buildings by using infrared thermography. *Buildings* **2019**, *9*, 32. [CrossRef]
12. Adamopoulos, E.; Volinia, M.; Girotto, M.; Rinaudo, F. Three-dimensional thermal mapping from IRT images for rapid architectural heritage NDT. *Buildings* **2020**, *10*, 187. [CrossRef]
13. Minkina, W.; Dudzik, S. *Infrared Thermography: Errors and Uncertainties*; John Wiley & Sons, Ltd.: Chichester, UK, 2009.
14. FLIR. The Ultimate Infrared Handbook for R&D Professionals. FLIR AB. 2012. Available online: https://www.flir.com/discover/rd-science/the-ultimate-infrared-handbook-for-rnd-professionals/ (accessed on 20 November 2021).
15. Tesař, J. *Thermography in Plasma and Laser Technologies*; University of West Bohemia: Pilsen, Czechia, 2014.
16. Budzier, H.; Gerlach, G. Calibration of uncooled thermal infrared cameras. *J. Sens. Sens. Syst.* **2015**, *4*, 187–197. [CrossRef]
17. Tesar, J.; Martan, J.; Skala, J. The influence of emissivity on measured temperature in dependence on spectral range of IR camera detector and its approximate calculation. *E-J. Nondestruct. Test.* **2016**, *22*, 840–841. [CrossRef]
18. Campbell, G.S.; Diak, G.R. Net and Thermal Radiation Estimation and Measurement. In *Micrometeorology in Agricultural Systems*; John Wiley & Sons, Inc.: Hoboken, NJ, USA, 2005; pp. 59–92.
19. Jonietz, F.; Myrach, P.; Suwala, H.; Ziegler, M. Examination of Spot Welded Joints with Active Thermography. *J. Nondestruct. Eval.* **2016**, *35*, 1. [CrossRef]
20. Myrach, P.; Jonietz, F.; Meinel, D.; Suwala, H.; Ziegler, M. Calibration of thermographic spot weld testing with X-ray computed tomography. *Quant. Infrared Thermogr. J.* **2017**, *14*, 122–131. [CrossRef]
21. Kastner, L.; Ahmadi, S.; Jonietz, F.; Jung, P.; Caire, G.; Ziegler, M.; Lambrecht, J. Classification of Spot-welded Joints in Laser Thermography Data using Convolutional Neural Networks. *IEEE Access* **2021**, *9*, 48303–48312. [CrossRef]